Growth hormone receptor (GHR) in AgRP neurons regulates thermogenesis in aged mice in a sex-specific manner

[1#]Lukas Stilgenbauer, [1#]Juliana Bezerra Medeiros de Lima, [1]Lucas Kniess Debarba, [1]Manal Khan, [1]Lisa Koshko, [2]John J. Kopchick, [3]Andrzej Bartke, [4]Augusto Schneider, *[1]Marianna Sadagurski

[1]Department of Biological Sciences, IBio (Integrative Biosciences Center), Wayne State University, Detroit, Michigan, MI, USA.
[2]Edison Biotechnology Institute, Ohio University, Athens, OH, USA
[3]Department of Internal Medicine, Southern Illinois University School of Medicine, Springfield, USA.
[4]Nutrition College, Federal University of Pelotas, Rio Grande do Sul, Brazil.

Running title: Hypothalamic growth hormone signaling controls body core temperature

Keywords: growth hormone receptor; thermoregulation; aging; AgRP neurons

[#] LS and JBL contributed equally to this study

***Corresponding author:**
Marianna Sadagurski,
Department of Biological Sciences,
Integrative Biosciences Center
Wayne State University
6135 Woodward, Detroit, MI 48202
Phone: (313) 577 8637
Email: sadagurski@wayne.edu

Abbreviations:

CNS, central nervous system; GH, growth hormone; GHR, growth hormone receptor; POMC, proopiomelanocortin; ARC, arcuate nucleus of the hypothalamus; DMH, dorsomedial hypothalamic nucleus; LHA, lateral hypothalamus; PVH, paraventricular hypothalamic nucleus; GHRH, growth hormone releasing hormone; AgRP, agouti-related peptide; BAT, brown adipose tissue

Abstract

Evidence for hypothalamic regulation of energy homeostasis and thermoregulation in brown adipose tissue (BAT) during aging has been well recognized, yet the central molecular mediators involved in this process are poorly understood. The arcuate hypothalamus (ARC), orexigenic agouti-related peptide (AgRP) neurons control nutrient intake, energy homeostasis, and BAT thermogenesis. To determine the roles of growth hormone receptor (GHR) signaling in the AgRP neurons we used mice with the AgRP-specific GHR deletion ($AgRP^{\Delta GHR}$). We found that female $AgRP^{\Delta GHR}$ mice were resistant to temperature adaptation, and their body core temperature remained significantly lower when held at 10°C, 22°C, or 30°C, compared to control mice. Low body core temperature in female $AgRP^{\Delta GHR}$ mice has been associated with significant reductions in *Ucp1* and *Pgc1α* expression in the BAT. Further, neuronal activity in AgRP in response to cold exposure was blunted in $AgRP^{\Delta GHR}$ females, while the number of Fos^{+} AgRP neurons was increased in control females exposed to cold. Global transcriptome from BAT identified increased expression of genes related to immune responses and chemokine activity and decreased expression of genes involved in triglycerides synthesis and metabolic pathways in $AgRP^{\Delta GHR}$ females. Importantly, these were the same genes that are downregulated by thermoneutrality in control mice but not in the $AgRP^{\Delta GHR}$ animals. Collectively, these data demonstrate a novel circuit of thermal regulation between the hypothalamic AgRP-GHR and BAT and provide insight into the brain systems that are critical for the thermogenic vitality of the elderly.

Introduction

During aging, BAT loses its thermogenic capacity and adaptation to cold temperatures thus reducing its ability to maintain normal energy homeostasis and body temperature late in life [1]. Energy homeostasis and thermoregulation are coordinated in the arcuate nucleus of the hypothalamus (ARC), which integrates neuronal and hormonal signals originating from peripheral tissues [2]. In the ARC, an antagonistic interaction between neurons expressing agouti-related peptide (AgRP) and neurons expressing proopiomelanocortin (POMC) constitutes the central metabolic controlling axis, and alterations in its activity impair energy homeostasis, thermoregulation, and peripheral glucose metabolism [3, 4]. Age-associated alterations in thermoregulation include low heat production, impaired thermal perception, and impaired autonomic and thermoregulatory responses [5]. Shivering is critical for heat production in a cold environment. Compared to young adults, shivering to increase heat production is impaired in elderly people and in laboratory animals, which reduces their tolerance for cold environments [6, 7].

In the hypothalamus, thermoregulatory circuits are modulated by leptin- and insulin-sensing neurons that respond to external nutrient and temperature cues [8]. Hypothalamic leptin and insulin signaling influence baselines of body core temperature in the fed state and oppose entry into a torpor-like state, without an effect on thermogenic response to cold [8]. In general, the preoptic area (POA) of the hypothalamus is responsible for managing body temperature, however, a subset of AgRP neurons was recently identified to mediate thermogenesis [9, 10]. In support, female mice lacking corticotropin-releasing factor receptor type 1 (CRFR1) selectively in AgRP neurons, exhibit a maladaptive thermogenic response to cold following impaired activation of the sympathetic nervous system (SNS) [11].

Growth hormone (GH) is a key mediator of growth and metabolism [12, 13]. GH deficient, long-lived Ames dwarf mice have highly active BAT compared to their littermates as indicated by depleted lipid stores, increased BAT tissue weight, increased expression of genes related to thermogenesis and lipid metabolism, and increased oxygen consumption and energy expenditure [14-16]. Housing Ames dwarf mice at thermoneutrality normalizes their lipid stores, gene expression, and oxygen consumption to those of control mice [14, 15], suggesting that BAT contributes to the extended longevity of GH-deficient mice.

GH activates AgRP neurons [17]. We and others have shown that young mice carrying AgRP-specific GHR ablation ($AgRP^{\Delta GHR}$ mice) have similar body weight, food intake, hormonal levels, and insulin sensitivity compared to control animals [17, 18]. However, during fasting AgRP

neurons' ability to save energy is impaired in AgRP GHR KO male mice, leading to increased fat loss, indicating GH as a starvation signal in AgRP neurons [17]. Given the role GH signaling plays in aging and its effect on BAT thermogenic capacity, in the current study we used AgRP$^{\Delta GHR}$ mice to explore the role of GHR signals in AgRP neurons in thermoregulation and thermoregulatory responses to temperature cues in aging animals.

Materials and Methods

Animals: Adult male and female AgRP$^{tm1(cre)}$ (AgRP-Ires-cre, stock 012899) were purchased from The Jackson Laboratory, and GHR$^{L/L}$ mice were described previously [19]. The characterization of the AgRP$^{\Delta GHR}$ mice was described previously [18]. We used wild-type littermate controls whenever possible and if not available, we used age-matched controls from the same breeding line. All mice were provided *ad libitum* access to a standard chow diet (Purina Lab Diet 5001) and housed in temperature-controlled rooms on a 12-hour/12-hour light-dark cycle. Procedures involved in this study were approved by the Wayne State University Institutional Animal Care and Use Committee (IACUC).

Temperature Exposure and Core Body Temperature Monitoring: Mice were anesthetized using isoflurane. A mid-sagittal incision was made in the abdomen and a passive RFID chip was inserted into the abdominal fat pat. Mice were monitored three times daily with RFID readers for core body temperature. Mice were housed at 22°C for two days before the temperature challenge to allow them to equilibrate. After two days of equilibration, the mice were then monitored for two days at 22°C followed by 3 days at 10°C, two days at 22°C, and three days at 30°C. Metabolic measurements of energy homeostasis at 22°C were obtained using an indirect calorimetry system (PhenoMaster, TSE system, Bad Homburg, Germany). The mice were acclimatized to the cages for 2 days and monitored for 5 days while food and water were provided *ad libitum*.

Perfusion and immunolabeling: Mice were anesthetized and perfused using phosphate buffer saline (PBS) (pH 7.5) followed by 4% paraformaldehyde (PFA). Brains were post-fixed, dehydrated, and sectioned coronally (30µm) using a sliding microtome, followed by immunofluorescent analysis as described [20]. For immunohistochemistry brain sections were washed with PBS six times, blocked with 0.3% Triton X-100 and 3% normal donkey serum in PBS for 2h; then the staining was carried out with the mouse anti-cFos (anti-rabbit, 1:500, cat. number sc-52, Santa Cruz). Immunostaining brain sections were pretreated with 0.5% NaOH and 0.5% H_2O_2 in PBS for 20 min. After the primary antibody, brain sections were incubated with AlexaFluor-

conjugated secondary antibodies for 2h (Invitrogen). Microscopic images of the stained sections were obtained using an Olympus FluoView 500 and Laser Scanning Confocal Microscope Zeiss LSM 800.

Quantification: For the quantification of immunoreactivity, images of matched brain areas were taken from at least 3 sections containing the hypothalamus for each brain between bregma -0.82 mm to -2.4 mm (according to the Franklin mouse brain atlas). Serial brain sections were made at 30 µm thickness, and every five sections were represented by one section with staining and cell counting. All sections were arranged from rostral to caudal to examine the distribution of labeled cells. $cFos^+$ cells were counted using ImageJ with DAPI (nuclear staining). The average of the total number of cells/field was assessed by statistical analysis as detailed below.

Quantitative Real-Time PCR: Total RNA was isolated from dissected BAT using Trizol reagent (Invitrogen, #15596026). The concentration of 1000 ng of RNA was used for cDNA synthesis using a High Capacity cDNA Reverse Transcription Kit (BioRad, #1708891). To detect the contaminated DNA we used the samples processed without the transcriptase reverse enzyme as negative controls. Quantitative real-time PCR was performed using the Applied Biosystems 7500 Real-Time PCR System. PGC1α, Forward: GCAACATGCTCAAGCCAAAC, Reverse: TGCAGTTCCAGAGAGTTCCA; Ucp1, Forward: GCTTTGCCTCACTCAGGATTGG, Reverse: CCAATGAACACTGCCACACCTC; FGF21, Forward: CCTCTAGGTTTCTTTGCCAACAG, Reverse: AAGCTGGCCTCAGGAT. Each PCR reaction was performed in duplicate. As negative controls, we used water instead of the cDNA, and ß-actin was measured in each cDNA sample as the housekeeping gene. The ΔΔCT method was used to determine the gene transcripts in each sample. For each sample, the threshold cycle (CT) was measured and normalized to the average of the housekeeping gene (ΔCT = CT gene of interest - CT housekeeping gene). The fold change of mRNA in the rest of the samples relative to the control male group was determined by 2-ΔΔCT. Data are shown as mRNA expression levels relative to the control males.

Histology and Morphometric Analysis: Histological analysis was performed on BAT tissues isolated from the animals at room temperature or exposed to 10°C, or at 30°C as previously described [21]. Morphometric analysis of BAT was performed with NIH ImageJ software (http://rsb.info.nih.gov/ij/).

RNA Extraction and mRNA sequencing: RNA-Seq was performed at the WSU Genome Sciences Core. All RNA-Seq data processing was performed as before [22]. Transcriptomic profile of individual BAT samples was performed using commercial RNA-sequencing kits

(NEBNext mRNA Library Prep Master Mix and NEBNext Multiplex Oligos for Illumina, New England Biolabs, Ipswich, MA) and adapted according to previous descriptions [22]. All RNA-Seq data are available at the Sequence Read Archive (SRA) at NCBI under accession number PRJNA871915. The mapping of sequencing reads to the mouse transcriptome and mRNA abundance was performed as previously [22]. mRNAs were further processed for pathway analysis using the Generally Applicable Gene-set Enrichment (GAGE), for the enrichment of KEGG pathways and gene ontology (GO) terms (biological processes, molecular function, and cellular component).

Statistical analysis: Statistical analyses for differentially expressed mRNAs were performed pairwise using EdgeR in the software R (3.2.2). Genes with a false discovery rate (FDR) < 0.05 and fold change (FC) > 2.0 were considered upregulated and with FDR < 0.05 and FC < 0.5 were considered downregulated. For all other experiments, the unpaired two-tailed Student's *t*-test was used for comparisons between two groups. Statistical analyses were performed using the GraphPad Prism software. A *p*-value of less than 0.05 was considered statistically significant.

Results

Female AgRP$^{\Delta GHR}$ mice exhibit decreased body core temperature. AgRP$^{\Delta GHR}$ mice show no difference in body weight as compared to control littermates (Figure 1A). Although, by 14 months of age female AgRP$^{\Delta GHR}$ mice demonstrated a slight, but insignificant (p=0.056), gain in body weight (Figure 1A). By 12 weeks of age, female but not male AgRP$^{\Delta GHR}$ mice exhibited reduced body core temperature compared to controls (Figures 1B and C). The body core temperature was overall higher in female mice, consistent with previous reports [23]. Additionally, when placed in metabolic chambers, female AgRP$^{\Delta GHR}$ mice exhibited a reduction in heat production without differences in the respiratory exchange ratio (RER) or ambulatory activity levels (Figure 1D and Supplementary Figure 1). These data are in agreement with a previous report showing that young AgRP$^{\Delta GHR}$ male mice exhibited no differences in heat production, RER or activity levels (Figure 1E and Supplementary Figure 1) [17]. Gene expression analysis of BAT demonstrated reduced levels of *Ucp1* (mitochondrial uncoupling protein 1) and *Pgc1α* (Ppargc1α, peroxisome proliferator-activated receptor gamma, coactivator 1 alpha) in 3 months old female AgRP$^{\Delta GHR}$ mice compared to control littermates (Figure 1F). We did not detect differences in the expression levels of *Ucp1* and *Pgc1α* in male AgRP$^{\Delta GHR}$ mice compared to controls (Figure 1G).

Interestingly, as found at a young age, 12-14 month-old female AgRP$^{\Delta GHR}$ mice exhibited decreased body core temperature compared to control. No differences were detected in body core temperature in male AgRP$^{\Delta GHR}$ mice (Figure 1H and I). Histological examination of BAT (H&E-stained sections) revealed a significant increase in lipid droplet size in brown adipocytes in young and middle-aged female AgRP$^{\Delta GHR}$ (Figure 1J, K, and Supplementary Figure 1C, D).

Remodeling of BAT transcription in adult AgRP$^{\Delta GHR}$ female mice. To further investigate age-related aberrations in BAT we performed bulk RNA sequencing (RNA-seq) of the BAT from 14-months old female AgRP$^{\Delta GHR}$ mice and compared it to control females. Results of principal component analysis for the most variable genes and hierarchical clustering in BAT identified a clear separation for control vs AgRP$^{\Delta GHR}$ animals (Supplementary Figure 2). Volcano plot shows the main upregulated and downregulated genes in female AgRP$^{\Delta GHR}$ mice relative to the controls (Figure 2A). The complete list of regulated pathways is presented in Supplementary Tables 1-3. Of particular interest, the number of lipid metabolic pathways, including triglyceride metabolism, glycerolipid metabolism, acylglycerol biosynthesis, lipid and phospholipid biosynthesis, and isocitrate metabolism, were significantly downregulated in BAT from female AgRP$^{\Delta GHR}$ mice as compared to the controls (Figure 2B). Among the genes associated with lipid metabolic processes and glucose regulation *Apobec1, Cyp2e1, Gk, Malat1, Ankrd9, Kcnq1ot1, Slc12a2,* and *Lpl* were downregulated, while genes associated with fatty acids metabolism *Scd1* and *Scd2* were upregulated (Figure 2C).

AgRP$^{\Delta GHR}$ female mice do not adapt to changes in temperature. To further investigate the requirement of GHR in AgRP neurons for adaptation to cold or at thermoneutrality, we recorded body core temperature during the light cycle in middle-aged 12-14 months old females exposed for 3 days to 10ºC or 30ºC and compared the outcomes to those measured in mice housed at room temperature (22ºC) (Figure 3A). Using this exposure paradigm, we found that female AgRP$^{\Delta GHR}$ mice maintained their low body core temperature upon exposure to 10ºC, as compared to control (Figure 3B). Furthermore, 3 days of exposure to 30ºC did not normalize the body core temperature of female AgRP$^{\Delta GHR}$ that was maintained consistently lower than controls (Figure 3C). Middle-aged male AgRP$^{\Delta GHR}$ mice showed adaptation to changes in temperature that was similar to their control littermates (Figure 3D, E and Supplementary Figure 3). Total body weight was unaffected (data not shown), however, the sustained cold exposure or thermoneutrality resulted in pronounced changes in BAT morphology in control animals. H&E-stained BAT from female mice housed at ambient temperature had brown adipocytes with multiple small lipid droplets, while BAT from female AgRP$^{\Delta GHR}$ mice had significantly larger single lipid droplets

(Figure 3F and G). In contrast, H&E stained-BAT from cold-exposed control female mice showed much smaller brown adipocytes, and fewer lipid droplets than at 22ºC ($p<0.00001$ for effect of temperature), indicating that cold exposure induced a loss of lipid droplets in the brown adipocytes (Figure 3F). We did not detect significant cold-induced morphological changes in female AgRP$^{\Delta GHR}$ mice compared to controls (Figure 3F and H). Regardless, *Ucp1* and *Pgc1* expression levels increased with cold temperature in control but not in female AgRP$^{\Delta GHR}$ mice. Importantly, the expression levels of *Ucp1* and *Pgc1* were downregulated in the female AgRP$^{\Delta GHR}$ mice housed at room temperature and maintained low regardless of the temperature change (Figure 3I). Interestingly, expression levels of *Fgf21* were also significantly elevated in response to cold exposure in control mice, supporting its activation by cold [24], while *Fgf21* levels were significantly reduced in cold but elevated at 30ºC in female AgRP$^{\Delta GHR}$ mice, suggesting transcriptional dysregulation of *Fgf21* in BAT.

ARC neurons do not adapt to cold exposure in female AgRP$^{\Delta GHR}$ mice. A recent study demonstrated that mild cold exposure induces activation of cFos protein, a marker of neuronal activation in AgRP neurons [25]. We found that the total number of cFos^{+} neurons in the ARC was comparable in both control and AgRP$^{\Delta GHR}$ mice maintained at 22°C. However, the number of cFos^{+} neurons was significantly increased in response to cold exposure in control, but not in female AgRP$^{\Delta GHR}$ mice (Figures 4A and B). These data are in agreement with previous findings showing that short but not long-term exposure to thermoneutrality suppressed activation of AgRP neurons [25, 26]. The number of cFos^{+} neurons in mice of both genotypes housed at 30° was minimal and similar to those measured at 22°C (Figure 4B).

BAT transcriptome in thermoneutrality in aged female AgRP$^{\Delta GHR}$ mice. We next assessed the impact of GHR deletion from AgRP neurons on BAT transcriptome in animals adapted to thermoneutrality for 3 days as compared to animals housed at room temperature. A total of 51 genes were changed in BAT by 30ºC in female AgRP$^{\Delta GHR}$ mice, compared to 101 genes in control mice (false discovery rate [FDR] < 0.05, Figure 5A) suggesting different mechanisms of adaptation. The regulated pathways for control and AgRP$^{\Delta GHR}$ females are shown in Supplementary Material. Female AgRP$^{\Delta GHR}$ mice were less responsive to thermoneutrality, with reduced changes in pathways when adapted from 22ºC to 30ºC (Figure 5B). Surprisingly, we identified several lipid metabolic pathways that were uniquely downregulated in control animals in adaptation to thermoneutrality and in AgRP$^{\Delta GHR}$ compared to control mice at 22ºC (Figure 5B). Specifically, lipid biosynthesis, glycerolipid metabolism, and lipid oxidation pathways were among those uniquely downregulated in control animals in adaptation from 22ºC to 30ºC. In the AgRP$^{\Delta GHR}$

females, these pathways were already downregulated at 22ºC and did not change with adaptation from 22ºC to 30ºC (Figure 5B and C). Among the common genes downregulated in both control and AgRP$^{\Delta GHR}$ mice by adaptation to thermoneutrality were metabolic genes *Gk, Dio2, Ucp3, Ucp1, and Ankrd9* (Figure 5D). Importantly, the genes associated with lipid accumulation and glucose regulation (*Malat1, Ankrd9, Kcnq1ot1, Slc12a2, Peg3)* which were downregulated only in control females in adaptation to 30ºC, were also downregulated in female AgRP$^{\Delta GHR}$ mice at 22ºC compared to control mice (Figure 5E and F). These genes were not changed in the female AgRP$^{\Delta GHR}$ mice in adaptation to 30ºC (Figure 5F), suggesting the role of GHR in AgRP neurons for the adaptation of BAT lipid and glucose metabolism to environmental temperatures.

Discussion

We identified a unique role for GHR signaling in hypothalamic AgRP neurons in controlling thermal adaptation. Using previously characterized AgRP-specific GHR knockout mice [18], we show that GHR signaling in AgRP neurons regulates body core temperature in females but not in male mice. Importantly, middle-aged female AgRP$^{\Delta GHR}$ mice show impaired adaptation to cold or thermoneutrality with increased BAT lipids accumulation and aberrant transcriptomic signatures. Specifically, female AgRP$^{\Delta GHR}$ mice exhibited transcriptomic signatures of downregulated lipid metabolic genes that are similar to those of control females adapting to temperature change. This indicates that GHR signaling mediates the response to thermoneutrality in the AgRP neurons in a sex-specific manner.

The ARC is a major site for the integration of multiple nutritional and hormonal signals, which are central to the modulation of energy balance and temperature homeostasis [27]. Evidence for the importance of GH-responsive neurons in the hypothalamus in energy homeostasis and nutrient deprivation was previously reported [18, 28-30]. Moreover, the orexigenic effect of GH signaling is possibly mediated by AgRP neurons, since most of the AgRP/NPY neurons express GHR, and AgRP-specific GHR-knockout mice are unable to adapt to food restriction and maintained a higher energy expenditure, having increased weight loss during food restriction compared to the control mice [17]. In support, our earlier study with young male and female AgRP$^{\Delta GHR}$ mice do not show changes in body weight, body composition, food intake, or glucose homeostasis [18]. Here we show that despite similar body weights and activity levels, the obligatory energy expenditure required for basal activity is reduced in young AgRP$^{\Delta GHR}$ female, but not male mice and is associated with lower body core temperature, reduced heat

production, increased BAT adipocytes size, and reduced BAT expression of thermogenic genes. During the aging process, such metabolic imbalance led to a slight increase in middle-aged females' body weight, accompanied by an inability to properly respond to changes in environmental temperatures. Given a significant increase in BAT lipids accumulation, the duration of eating/fasting patterns may be different in AgRP$^{\Delta GHR}$ female mice since AgRP neurons regulate complex behavioral and physiological feeding changes [31, 32]. It is reasonable to hypothesize that age-associated decline in GH signaling in the AgRP neurons is responsible for or importantly contributes to the impairment in BAT thermogenic capacity occurring with age in female mice [33].

Recent work has established that in addition to negative feedback regulation of hormonal signals to nutrient intake and energy metabolism, AgRP neuron activity rapidly increases following exposure to a mild cold environment and that the activity of these neurons at thermoneutrality is lower [25]. Moreover, exposure to a warm environment was shown to suppress AgRP activity in 10-day-old pups [26]. A recent study demonstrated that the control of BAT thermogenesis by AgRP neurons is independent of environmental temperature and activation of thermoregulation since specific activation of AgRP neurons suppresses BAT thermogenic activity [34]. Specifically, in mice maintained in the thermoneutral zone of 30°C, the effects of AgRP neuronal activation on BAT temperature, energy expenditure, and locomotor activity were significantly reduced. Moreover, during cold exposure, chemogenetic activation of AgRP neurons reduced BAT temperature to a similar extent as at ambient temperature, providing evidence for the AgRP-BAT circuit independent of environmental temperature and cold-induced thermoregulation. This effect was mediated via hypothalamic mTOR complex-1 (mTORC1) signaling [34].

Middle-aged AgRP$^{\Delta GHR}$ female mice exhibit reduced body core temperature regardless of environmental temperature (22°C, 10°C, or 30°C), suggesting that GHR signaling in the AgRP neurons, can sense energy availability and AgRP activity related to AgRP-BAT circuit. mTORC1 activity is indeed lower in multiple organs of Snell dwarf and global GHRKO mice [35], suggesting a requirement of this mechanism and properly regulated GHR signaling in AgRP neurons for thermogenic action. Indeed, we found down regulation of mTOR signaling in control BAT but not in BAT of AgRP$^{\Delta GHR}$ females. Further insights on the regulation of the mTORC1 pathway in the AgRP neurons lacking GHR signaling would be informative to establish the role of this circuit in the regulation of body core temperature in aging.

Our new data provide critical insight into the sexual dimorphism of GHR signals in AgRP neurons in thermoregulation. While unexpected, a similar sex-specific phenotype was shown in females lacking corticotropin-releasing factor receptor type 1 (CRFR1) in AgRP neurons [11].

Only female mice selectively lacking CRFR1 in AgRP neurons exhibited reduced heat production, and lower body temperature, followed by a maladaptive thermogenic response to cold. In the ARC, the GHR gene is co-expressed with CRFR in the same cluster of AgRP neurons [36], suggesting a sex-specific role of this subpopulation of AgRP neurons in energy homeostasis and regulation of body core temperature. Additionally, a sex-specific phenotype was observed in females lacking leptin receptors in POMC neurons or AgRP neurons, which, as in AgRP$^{\Delta GHR}$ and AgRP$^{\Delta CRFR1}$ females, exhibited reduced heat production with unaltered food intake [37, 38]. These sex-specific differences can be attributed to hypothalamic estrogen signals [39]. There is some evidence that estrogen modulates GH action independent of secretion [40]. While estrogen receptor is not expressed by AgRP neurons [41], estrogen can directly affect GHR expression and signaling [40]. However, it is important to note that within each sex, the levels of GH, were unaltered in AgRP$^{\Delta GHR}$ mice [17, 18]. Our new studies thus provide a critical view of the sex-specific role of GHR signaling in AgRP neurons in thermoregulation with particular importance for aged females.

Transcriptomic analysis of BAT demonstrated that genes associated with lipid metabolic processes and lipids accumulation were downregulated in AgRP$^{\Delta GHR}$ compared to control. Moreover, these were the same genes downregulated by thermoneutrality in control mice but not in the AgRP$^{\Delta GHR}$ animals. The divergent response of BAT in the AgRP$^{\Delta GHR}$ females was evident by downregulation in key genes associated with lipid accumulation and glucose regulation such as *Malat1, Ankrd9, Kcnq1ot1, Slc12a2, and Peg3.* These genes were not changed in the AgRP$^{\Delta GHR}$ females during adaptation to 30ºC. Some of these genes, such as *Malat1* were shown to promote hepatic steatosis and insulin resistance by modulating lipid accumulation through SREBP-1c [42], while *Ankrd9*, *Kcnq1ot1*, *Peg3* are involved in intracellular lipid accumulation, and lipogenesis [43-45], and *Slc12a2* plays a role in insulin secretion and glucose-stimulated plasma membrane depolarization [46]. This selective alteration in the genes is regulated by the acclimation to a thermoneutral environment in middle-age control females resembles the changes detected in the AgRP$^{\Delta GHR}$ mice at 22ºC. This suggests that these animals were capable of maintaining the basal metabolic rate of low euthermia thought their life span regardless of the temperature exposure. Interestingly, genes associated with fatty acids metabolism *Scd1* and *Scd2* were upregulated in the AgRP$^{\Delta GHR}$ females indicating shifts in metabolic homeostasis and substrate utilization [47]. Interestingly, SCD1 deficiency stimulates basal thermogenesis through the upregulation of the beta-3-AR-mediated pathway and an increase in lipolysis and fatty acid oxidation in BAT [48].

A relationship between GH and thermoregulation was previously suggested. Central infusion of GH into the hypothalamus leads to an increase in sympathetic nerve activity [49, 50]. Furthermore, the inability of whole-body GHRKO mice to respond to cold exposure or β-adrenergic receptor agonist treatment suggested that GH plays an important role in thermoregulation [51]. Previous studies using whole-body GHRKO and GH deficient Ames dwarf mice, showed an increased amount of BAT [14, 52], increased expression of thermogenic genes in BAT, and thermogenic activation ('browning") of subcutaneous white adipose tissue (WAT), which can stimulate thermogenesis [53]. Intriguingly, similarly to AgRP$^{\Delta GHR}$ females, body core temperature was reduced in these mutants [54, 55] despite increased thermogenesis and metabolic rate. Reduced body temperature has been associated with extended longevity [56]. Additionally, GH-deficient mice exposed to thermoneutrality had reduced expression of genes associated with lipid metabolism and energy expenditure, and morphological changes in BAT similar to AgRP$^{\Delta GHR}$ females [22]. More than 1500 genes are regulated in BAT at room temperature or thermoneutrality in global GHRKO mice [22]. When GHRKO mice were exposed to thermoneutral conditions, a greater number of genes were affected in BAT from GHRKO than control mice, with low overlap between groups, indicating a divergent response. Similar to the global GHRKO mice, AgRP$^{\Delta GHR}$ mice, showed little overlap in genes when compared to the responses of control mice to thermoneutrality. Nevertheless, 114 genes were commonly regulated in response to thermoneutrality by global GHRKO and AgRP$^{\Delta GHR}$. Among the pathways regulated by these common genes, lipid metabolic process, fatty acid metabolic process, response to cold, and brown fat cell differentiation were the top regulated GO terms [22]. Similarly to AgRP$^{\Delta GHR}$ mice, *Ankrd9* was upregulated in GHRKO mice at 22ºC but downregulated in GHRKO mice exposed to thermoneutral conditions [22]. On the other hand, *Peg3* was upregulated in GHRKO compared to WT mice at 22ºC, while *Slc12a2* and *Scd1* were downregulated in GHRKO mice exposed to thermoneutrality [22], reflecting the differences between both models. Additional work will be required to define the common and divergent responses between these models in the regulation of body core temperature and energy homeostasis.

Aging is associated with an attenuated physiological ability to maintain body core temperature and the risk of heat-related illness in these individuals is elevated [57]. The role of sex and reproductive hormones in thermoregulation is complex and depends on the situation, overall health, and age [58]. Our data provide evidence that GHR signaling in the AgRP neurons mediates the response to thermoneutrality, controlling lifetime steady state temperature in female animals. Future studies would be required to define the impact of low body core temperature in AgRP$^{\Delta GHR}$ female mice on longevity and metabolic health in aging.

Author contribution

LS, JBML, LKD, carried out the research and reviewed the manuscript. MK and LK assisted in data collection and experimental design. JJK contributed the GHR flox mice. AS and AB analyzed the data and reviewed the manuscript. MS designed the study, analyzed the data, wrote the manuscript, and is responsible for the integrity of this work. All authors approved the final version of the manuscript.

Funding

This study was supported by the American Diabetes Association grant #1-IB-IDF-063, a Feasibility Grant from the Michigan Diabetes Research Center (P30DK020572) NIDDK, by MICP Core and metabolic core (P30DK020572) NIDDK and WSU funds for MS.

Disclosure

No conflicts of interest are declared by the authors.

Data Availability Statement

The data that support the findings of this study are available from the corresponding author upon reasonable request.

REFERENCES

1. Mattson, M.P., *Perspective: Does brown fat protect against diseases of aging?* Ageing Res Rev, 2010. **9**(1): p. 69-76.
2. Roh, E. and M.S. Kim, *Brain Regulation of Energy Metabolism.* Endocrinol Metab (Seoul), 2016. **31**(4): p. 519-524.
3. Robertson, S.A., G.M. Leinninger, and M.G. Myers, Jr., *Molecular and neural mediators of leptin action.* Physiol Behav, 2008. **94**(5): p. 637-642.
4. Belgardt, B.F. and J.C. Bruning, *CNS leptin and insulin action in the control of energy homeostasis.* Ann N Y Acad Sci, 2010. **1212**: p. 97-113.
5. Van Someren, E.J., *Thermoregulation and aging.* Am J Physiol Regul Integr Comp Physiol, 2007. **292**(1): p. R99-102.
6. Osilla, E.V., J.L. Marsidi, and S. Sharma, *Physiology, Temperature Regulation*, in *StatPearls*. 2022: Treasure Island (FL).
7. Rosenbaum, M. and R.L. Leibel, *Adaptive thermogenesis in humans.* Int J Obes (Lond), 2010. **34 Suppl 1**: p. S47-55.
8. Chong, A.C., R.A. Greendyk, and L.M. Zeltser, *Distinct networks of leptin- and insulin-sensing neurons regulate thermogenic responses to nutritional and cold challenges.* Diabetes, 2015. **64**(1): p. 137-46.
9. Han, Y., et al., *Deciphering an AgRP-serotoninergic neural circuit in distinct control of energy metabolism from feeding.* Nat Commun, 2021. **12**(1): p. 3525.
10. Yu, S., et al., *The Hypothalamic Preoptic Area and Body Weight Control.* Neuroendocrinology, 2018. **106**(2): p. 187-194.
11. Kuperman, Y., et al., *CRFR1 in AgRP Neurons Modulates Sympathetic Nervous System Activity to Adapt to Cold Stress and Fasting.* Cell Metab, 2016. **23**(6): p. 1185-99.
12. Bartke, A. and H. Brown-Borg, *Life extension in the dwarf mouse.* Curr. Top. Dev. Biol, 2004. **63**: p. 189-225.
13. Waters, M.J., et al., *New insights into growth hormone action.* J. Mol. Endocrinol, 2006. **36**(1): p. 1-7.
14. Darcy, J., et al., *Brown Adipose Tissue Function Is Enhanced in Long-Lived, Male Ames Dwarf Mice.* Endocrinology, 2016. **157**(12): p. 4744-4753.
15. Darcy, J., et al., *Increased environmental temperature normalizes energy metabolism outputs between normal and Ames dwarf mice.* Aging (Albany NY), 2018. **10**(10): p. 2709-2722.
16. Westbrook, R., et al., *Alterations in oxygen consumption, respiratory quotient, and heat production in long-lived GHRKO and Ames dwarf mice, and short-lived bGH transgenic mice.* J Gerontol A Biol Sci Med Sci, 2009. **64**(4): p. 443-51.
17. Furigo, I.C., et al., *Growth hormone regulates neuroendocrine responses to weight loss via AgRP neurons.* Nat Commun, 2019. **10**(1): p. 662.
18. de Lima, J.B.M., et al., *Hypothalamic GHR-SIRT1 Axis in Fasting.* Cells, 2021. **10**(4).
19. List, E.O., et al., *Liver-specific GH receptor gene-disrupted (LiGHRKO) mice have decreased endocrine IGF-I, increased local IGF-I, and altered body size, body composition, and adipokine profiles.* Endocrinology, 2014. **155**(5): p. 1793-805.
20. Sadagurski, M., G. Cady, and R.A. Miller, *Anti-aging drugs reduce hypothalamic inflammation in a sex-specific manner.* Aging Cell, 2017. **16**(4): p. 652-660.
21. Sadagurski, M., et al., *Human IL6 enhances leptin action in mice.* Diabetologia, 2010. **53**(3): p. 525-535.

22. Schneider, A., et al., *Growth Hormone Signaling Shapes the Impact of Environmental Temperature on Transcriptomic Profile of Different Adipose Tissue Depots in Male Mice.* The Journals of Gerontology: Series A, 2021. **77**(5): p. 941-946.
23. Sanchez-Alavez, M., S. Alboni, and B. Conti, *Sex- and age-specific differences in core body temperature of C57Bl/6 mice.* Age (Dordr), 2011. **33**(1): p. 89-99.
24. Klein Hazebroek, M. and S. Keipert, *Adapting to the Cold: A Role for Endogenous Fibroblast Growth Factor 21 in Thermoregulation?* Front Endocrinol (Lausanne), 2020. **11**: p. 389.
25. Deem, J.D., et al., *Cold-induced hyperphagia requires AgRP neuron activation in mice.* Elife, 2020. **9**.
26. Zimmer, M.R., et al., *Functional Ontogeny of Hypothalamic Agrp Neurons in Neonatal Mouse Behaviors.* Cell, 2019. **178**(1): p. 44-59 e7.
27. Timper, K. and J.C. Bruning, *Hypothalamic circuits regulating appetite and energy homeostasis: pathways to obesity.* Dis Model Mech, 2017. **10**(6): p. 679-689.
28. de Lima, J.B.M., et al., *ARCGHR Neurons Regulate Muscle Glucose Uptake.* Cells, 2021. **10**(5): p. 1093.
29. Furigo, I.C., et al., *Growth hormone enhances the recovery of hypoglycemia via ventromedial hypothalamic neurons.* FASEB J, 2019: p. fj201901315R.
30. Wasinski, F., et al., *Growth Hormone Receptor Deletion Reduces the Density of Axonal Projections from Hypothalamic Arcuate Nucleus Neurons.* Neuroscience, 2020. **434**: p. 136-147.
31. Dietrich, M.O., et al., *Hypothalamic Agrp neurons drive stereotypic behaviors beyond feeding.* Cell, 2015. **160**(6): p. 1222-32.
32. Cavalcanti-de-Albuquerque, J.P., et al., *Regulation of substrate utilization and adiposity by Agrp neurons.* Nat Commun, 2019. **10**(1): p. 311.
33. Graja, A. and T.J. Schulz, *Mechanisms of Aging-Related Impairment of Brown Adipocyte Development and Function.* Gerontology, 2015. **61**(3): p. 211-217.
34. Burke, L.K., et al., *mTORC1 in AGRP neurons integrates exteroceptive and interoceptive food-related cues in the modulation of adaptive energy expenditure in mice.* Elife, 2017. **6**.
35. Dominick, G., et al., *Regulation of mTOR activity in Snell dwarf and GH receptor gene-disrupted mice.* Endocrinology, 2015. **156**(2): p. 565-75.
36. Campbell, J.N., et al., *A molecular census of arcuate hypothalamus and median eminence cell types.* Nat Neurosci, 2017. **20**(3): p. 484-496.
37. Shi, H., et al., *Sexually different actions of leptin in proopiomelanocortin neurons to regulate glucose homeostasis.* Am J Physiol Endocrinol Metab, 2008. **294**(3): p. E630-9.
38. van de Wall, E., et al., *Collective and individual functions of leptin receptor modulated neurons controlling metabolism and ingestion.* Endocrinology, 2008. **149**(4): p. 1773-1785.
39. Frank, A., L.M. Brown, and D.J. Clegg, *The role of hypothalamic estrogen receptors in metabolic regulation.* Front Neuroendocrinol, 2014. **35**(4): p. 550-7.
40. Leung, K.C., et al., *Estrogen regulation of growth hormone action.* Endocr Rev, 2004. **25**(5): p. 693-721.
41. Olofsson, L.E., A.A. Pierce, and A.W. Xu, *Functional requirement of AgRP and NPY neurons in ovarian cycle-dependent regulation of food intake.* Proc Natl Acad Sci U S A, 2009. **106**(37): p. 15932-7.
42. Yan, C., J. Chen, and N. Chen, *Long noncoding RNA MALAT1 promotes hepatic steatosis and insulin resistance by increasing nuclear SREBP-1c protein stability.* Sci Rep, 2016. **6**: p. 22640.
43. Wang, X., et al., *Regulation of ANKRD9 expression by lipid metabolic perturbations.* BMB Rep, 2009. **42**(9): p. 568-73.

44. Yu, X.H., et al., *LncRNA kcnq1ot1 promotes lipid accumulation and accelerates atherosclerosis via functioning as a ceRNA through the miR-452-3p/HDAC3/ABCA1 axis.* Cell Death Dis, 2020. **11**(12): p. 1043.
45. Ghimire, S. and J. Kim, *PEG3 controls lipogenesis through ACLY.* PLoS One, 2021. **16**(5): p. e0252354.
46. Alshahrani, S., et al., *Increased Slc12a1 expression in beta-cells and improved glucose disposal in Slc12a2 heterozygous mice.* J Endocrinol, 2015. **227**(3): p. 153-65.
47. Flowers, M.T. and J.M. Ntambi, *Role of stearoyl-coenzyme A desaturase in regulating lipid metabolism.* Curr Opin Lipidol, 2008. **19**(3): p. 248-56.
48. Lee, S.H., et al., *Lack of stearoyl-CoA desaturase 1 upregulates basal thermogenesis but causes hypothermia in a cold environment.* J Lipid Res, 2004. **45**(9): p. 1674-82.
49. Tran, L.T., et al., *Hypothalamic control of energy expenditure and thermogenesis.* Experimental & Molecular Medicine, 2022. **54**(4): p. 358-369.
50. Yasuda, T., et al., *Centrally administered ghrelin suppresses sympathetic nerve activity in brown adipose tissue of rats.* Neurosci Lett, 2003. **349**(2): p. 75-8.
51. Nelson, C.N., et al., *Growth hormone activated STAT5 is required for induction of beige fat in vivo.* Growth Horm IGF Res, 2018. **42-43**: p. 40-51.
52. Li, Y., J.R. Knapp, and J.J. Kopchick, *Enlargement of interscapular brown adipose tissue in growth hormone antagonist transgenic and in growth hormone receptor gene-disrupted dwarf mice.* Exp Biol Med (Maywood), 2003. **228**(2): p. 207-15.
53. Desai, B.N. and R.B. Harris, *Integrated effects of leptin in the forebrain and hindbrain of male rats.* Endocrinology, 2013. **154**(8): p. 2663-75.
54. Hunter, W.S., et al., *Low body temperature in long-lived Ames dwarf mice at rest and during stress.* Physiol Behav, 1999. **67**(3): p. 433-7.
55. Hauck, S.J., et al., *Reduced levels of thyroid hormones, insulin, and glucose, and lower body core temperature in the growth hormone receptor/binding protein knockout mouse.* Exp Biol Med (Maywood), 2001. **226**(6): p. 552-8.
56. Conti, B., et al., *Transgenic mice with a reduced core body temperature have an increased life span.* Science, 2006. **314**(5800): p. 825-8.
57. Waalen, J. and J.N. Buxbaum, *Is older colder or colder older? The association of age with body temperature in 18,630 individuals.* J Gerontol A Biol Sci Med Sci, 2011. **66**(5): p. 487-92.
58. Yanovich, R., I. Ketko, and N. Charkoudian, *Sex Differences in Human Thermoregulation: Relevance for 2020 and Beyond.* Physiology, 2020. **35**(3): p. 177-184.

Legends:

Figure 1. Temperature control in AgRP$^{\Delta GHR}$ mice. (A) Body weight. Body core temperature of (B) 12-week-old female and (C) male control and AgRP$^{\Delta GHR}$ mice. Energy parameters were measured in *ad libitum* control and AgRP$^{\Delta GHR}$ mice. Heat production in (D) female and (E) male mice. Gene expression of *UCP1* and *PGC1* in BAT of 12-weeks old (F) female and (G) male mice (n=6). Data are shown as mean ± SEM. *, p<0.001. Body core temperature of 12-14 months old (H) female and (I) male control and AgRP$^{\Delta GHR}$ mice (n=7-8). Representative images (J) and quantification (K) of H&E staining in BAT of 12-14 months old female mice (n=6). Data are shown as mean ± SEM. *, p<0.05. See also Supplementary Figure 1.

Figure 2: BAT transcription profile in adult AgRP$^{\Delta GHR}$ female mice. (A) Volcano plot of differential expression genes in 12-14 months old AgRP$^{\Delta GHR}$ females compared to control females. The blue, red, and grey dots represent the down-regulated, up-regulated, and unchanged genes respectively. (B) Down-regulated functions identified by GO-analysis. (C) Network analysis of differentially expressed genes associated with carbohydrate metabolic process, lipid metabolic process, immune system, homeostatic process, and stress response. Red: up-regulated genes compared to the control group; blue: down-regulated genes compared to the control group. See also Supplementary Figure 2 and Supplementary Tables for pathways analysis.

Figure 3: Effect of cold exposure or thermoneutrality on body core temperature and BAT gene expression. (A) 12-14 month-old control and AgRP$^{\Delta GHR}$ females and males were housed in temperature-controlled chambers set to either cold (10°C) or 30ºC for 3 days. Body core temperature in (B) females and (D) males housed at 10°C. Body core temperature in (C) females and (E) males housed over 3 days at 30°C. n = 5–8 per group, mean ± SEM. Student's t-test, *, p<0.05. Representative images (F) and quantification (G and H) of H&E staining in BAT of 12-14 months old female mice housed at 10°C or 30ºC for 3 days (n=6), t-test *p<0.05, **p<0.01. See also Supplementary Figure 3 for H&E staining in BAT of 12-14 months old male mice. (I) Gene expression of *PGC1*, *UCP1,* and *Fgf21* in BAT of 12-14-month-old control and AgRP$^{\Delta GHR}$ females housed at 22°C, 10°C or 30°C as determined by qRT-PCR, mean ± SEM. Two-way ANOVA followed by Newman–Keuls test, *p<0.05, **p<0.01, ****p<0.0001 vs. 22°C.

Figure 4: Cold exposure activates ARC neurons in control but not in AgRP$^{\Delta GHR}$ females. (A) Representative images of immunohistochemical detection of cFos (red) the arcuate nucleus (ARC) of 12-14-month-old control and AgRP$^{\Delta GHR}$ females after housing at either 10°C, 22°C, or 30°C. (B) Quantitation of Fos positive cells in the ARC. Scale bar, 100 mm, n = 3–5 group, mean ± SEM. Two-way ANOVA followed by Newman–Keuls test, **p<0.01 vs. 22°C.

Figure 5: Differentially expressed genes in AgRP$^{\Delta GHR}$ females exposed to thermoneutrality. (A) The Venn diagram depicts the number of overlapping genes and differentially expressed genes between 12-14 month-old control and AgRP$^{\Delta GHR}$ females (left) at 30°C versus 22°C. (B) Down-regulated functions were identified by GO-analysis in control females at 30°C versus 22°C. (C) Down-regulated functions were identified by GO-analysis in AgRP$^{\Delta GHR}$ females at 30°C versus 22°C. (D) Heatmap illustrating the relative expression of overlapping genes by 30°C. (E) Genes regulated only in control females (right) or only in AgRP$^{\Delta GHR}$ females (left) at 30ºC vs 22ºC. (F) Heatmap illustrating the differentially expressed genes in AgRP$^{\Delta GHR}$ females at 22ºC vs control, and the relative expression of unique genes at 30ºC vs 22ºC in control and AgRP$^{\Delta GHR}$ females.

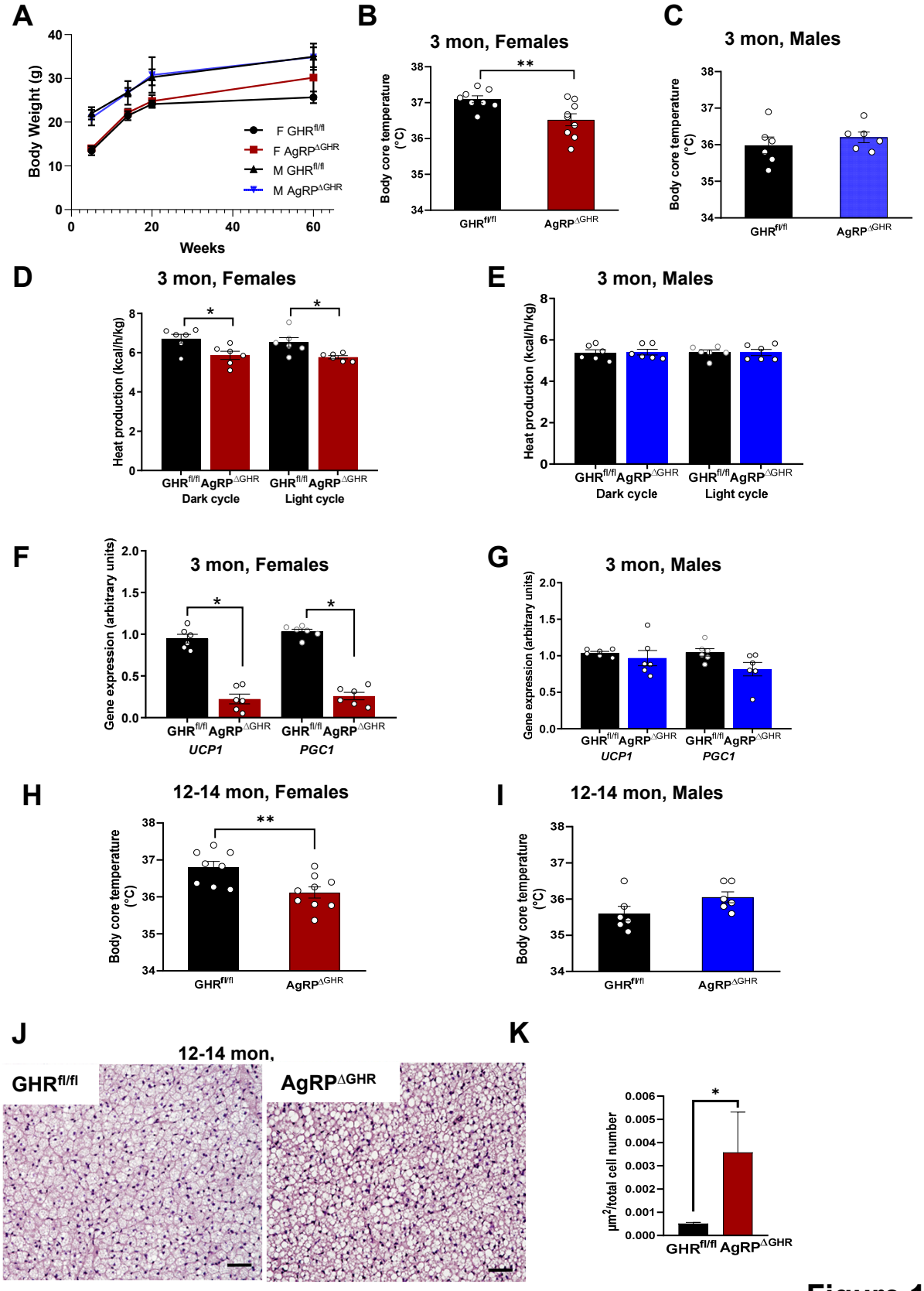
A
Body Weight (g)
Weeks
F GHR$^{fl/fl}$
F AgRP$^{\Delta GHR}$
M GHR$^{fl/fl}$
M AgRP$^{\Delta GHR}$
B
3 mon, Females
Body core temperature (°C)
GHR$^{fl/fl}$
AgRP$^{\Delta GHR}$
C
3 mon, Males
D
3 mon, Females
Heat production (kcal/h/kg)
Dark cycle
Light cycle
E
3 mon, Males
F
3 mon, Females
Gene expression (arbitrary units)
UCP1
PGC1
G
3 mon, Males
H
12-14 mon, Females
I
12-14 mon, Males
J
12-14 mon,
GHR$^{fl/fl}$
AgRP$^{\Delta GHR}$
K
µm^2/total cell number

Figure 1

A

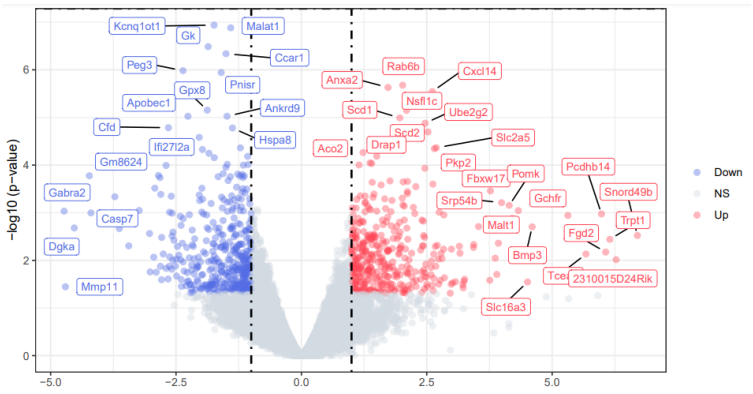
Kcnq1ot1
Gk
Malat1
Ccar1
Peg3
Pnisr
Gpx8
Apobec1
Ankrd9
Cfd
Hspa8
Ifi27l2a
Gm8624
Gabra2
Casp7
Dgka
Mmp11
Rab6b
Cxcl14
Anxa2
Nsfl1c
Scd1
Ube2g2
Scd2
Slc2a5
Aco2
Drap1
Pkp2
Pcdhb14
Fbxw17
Pomk
Snord49b
Srp54b
Gchfr
Trpt1
Malt1
Fgd2
Bmp3
Tce
2310015D24Rik
Slc16a3
−log10 (p−value)
−5.0
−2.5
0.0
2.5
5.0
0
2
4
6
Down
NS
Up

B

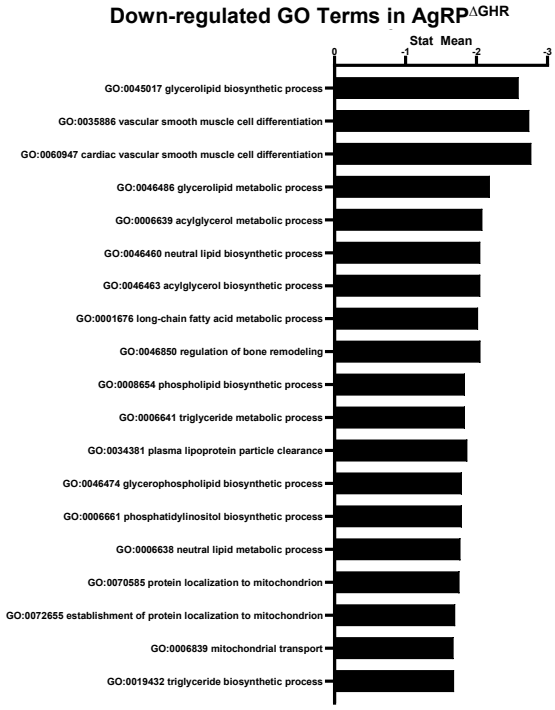
Down-regulated GO Terms in AgRP$^{\Delta GHR}$
Stat Mean
0
-1
-2
-3
GO:0045017 glycerolipid biosynthetic process
GO:0035886 vascular smooth muscle cell differentiation
GO:0060947 cardiac vascular smooth muscle cell differentiation
GO:0046486 glycerolipid metabolic process
GO:0006639 acylglycerol metabolic process
GO:0046460 neutral lipid biosynthetic process
GO:0046463 acylglycerol biosynthetic process
GO:0001676 long-chain fatty acid metabolic process
GO:0046850 regulation of bone remodeling
GO:0008654 phospholipid biosynthetic process
GO:0006641 triglyceride metabolic process
GO:0034381 plasma lipoprotein particle clearance
GO:0046474 glycerophospholipid biosynthetic process
GO:0006661 phosphatidylinositol biosynthetic process
GO:0006638 neutral lipid metabolic process
GO:0070585 protein localization to mitochondrion
GO:0072655 establishment of protein localization to mitochondrion
GO:0006839 mitochondrial transport
GO:0019432 triglyceride biosynthetic process

C

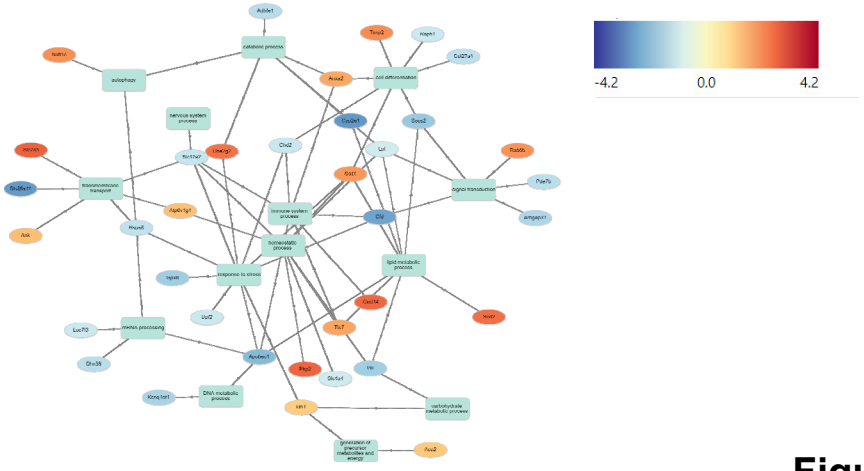
-4.2
0.0
4.2

Figure 2

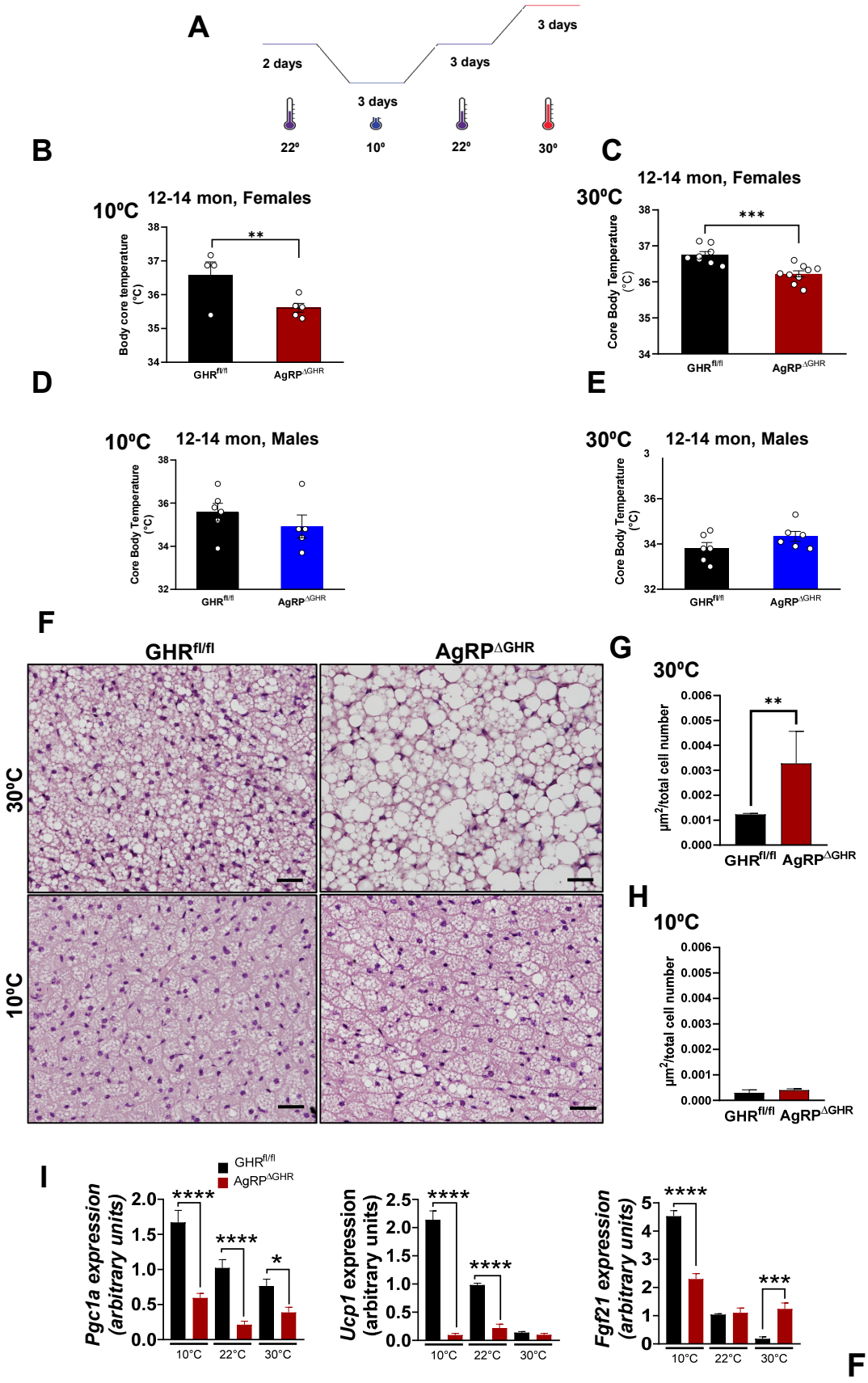
A
2 days
3 days
3 days
3 days
22º
10º
22º
30º
B
10ºC
12-14 mon, Females
Body core temperature (ºC)
**
GHRfl/fl
AgRPΔGHR
C
30ºC
12-14 mon, Females
Core Body Temperature (ºC)
***
GHRfl/fl
AgRPΔGHR
D
10ºC
12-14 mon, Males
Core Body Temperature (ºC)
GHRfl/fl
AgRPΔGHR
E
30ºC
12-14 mon, Males
Core Body Temperature (ºC)
GHRfl/fl
AgRPΔGHR
F
GHRfl/fl
AgRPΔGHR
30ºC
10ºC
G
30ºC
µm2/total cell number
**
GHRfl/fl
AgRPΔGHR
H
10ºC
µm2/total cell number
GHRfl/fl
AgRPΔGHR
I
GHRfl/fl
AgRPΔGHR
Pgc1a expression (arbitrary units)
****
****
*
10°C
22°C
30°C
Ucp1 expression (arbitrary units)
****
****
10°C
22°C
30°C
Fgf21 expression (arbitrary units)
****
***
10°C
22°C
30°C

Figure 3

A

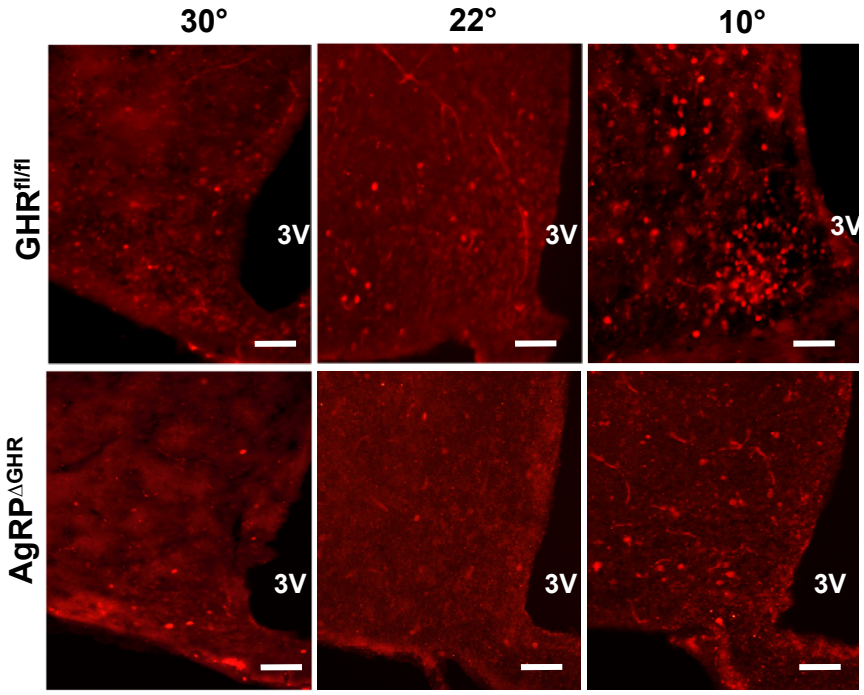
30°
22°
10°
GHRfl/fl
AgRPΔGHR
3V

B

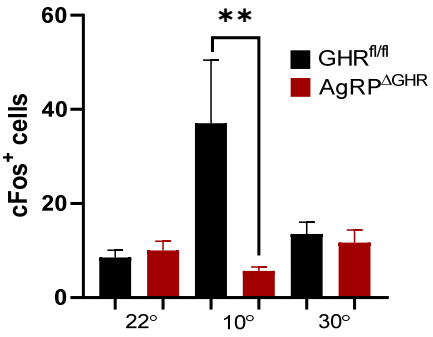
60
40
20
0
cFos+ cells
**
GHRfl/fl
AgRPΔGHR
22°
10°
30°

Figure 4

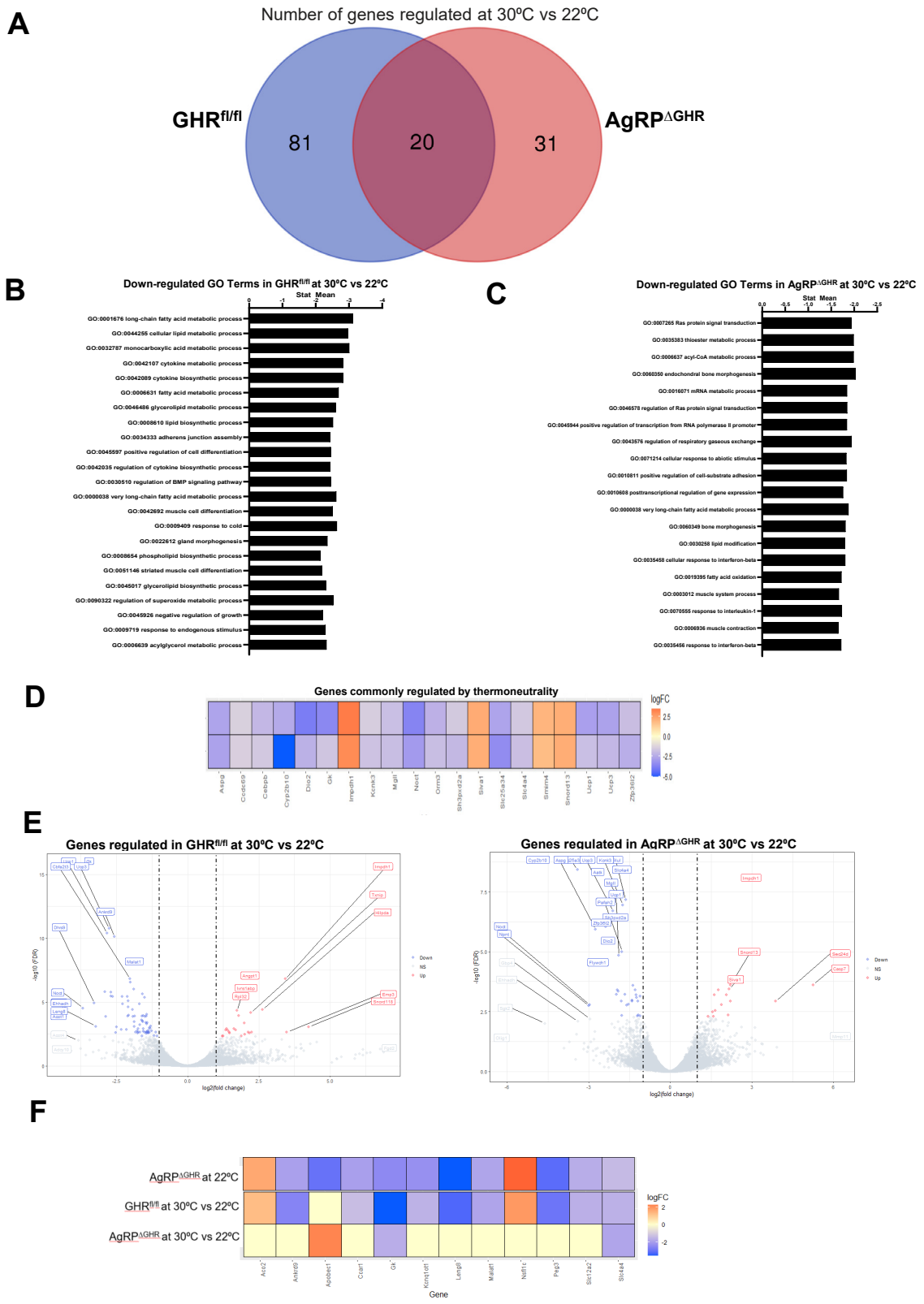
A
Number of genes regulated at 30ºC vs 22ºC
GHRfl/fl
81
20
31
AgRPΔGHR
B
Down-regulated GO Terms in GHRfl/fl at 30ºC vs 22ºC
Stat Mean
GO:0001676 long-chain fatty acid metabolic process
GO:0044255 cellular lipid metabolic process
GO:0032787 monocarboxylic acid metabolic process
GO:0042107 cytokine metabolic process
GO:0042089 cytokine biosynthetic process
GO:0006631 fatty acid metabolic process
GO:0046486 glycerolipid metabolic process
GO:0008610 lipid biosynthetic process
GO:0034333 adherens junction assembly
GO:0045597 positive regulation of cell differentiation
GO:0042035 regulation of cytokine biosynthetic process
GO:0030510 regulation of BMP signaling pathway
GO:0000038 very long-chain fatty acid metabolic process
GO:0042692 muscle cell differentiation
GO:0009409 response to cold
GO:0022612 gland morphogenesis
GO:0008654 phospholipid biosynthetic process
GO:0051146 striated muscle cell differentiation
GO:0045017 glycerolipid biosynthetic process
GO:0090322 regulation of superoxide metabolic process
GO:0045926 negative regulation of growth
GO:0009719 response to endogenous stimulus
GO:0006639 acylglycerol metabolic process
C
Down-regulated GO Terms in AgRPΔGHR at 30ºC vs 22ºC
Stat Mean
GO:0007265 Ras protein signal transduction
GO:0035383 thioester metabolic process
GO:0006637 acyl-CoA metabolic process
GO:0060350 endochondral bone morphogenesis
GO:0016071 mRNA metabolic process
GO:0046578 regulation of Ras protein signal transduction
GO:0045944 positive regulation of transcription from RNA polymerase II promoter
GO:0043576 regulation of respiratory gaseous exchange
GO:0071214 cellular response to abiotic stimulus
GO:0010811 positive regulation of cell-substrate adhesion
GO:0010608 posttranscriptional regulation of gene expression
GO:0000038 very long-chain fatty acid metabolic process
GO:0060349 bone morphogenesis
GO:0030258 lipid modification
GO:0035458 cellular response to interferon-beta
GO:0019395 fatty acid oxidation
GO:0003012 muscle system process
GO:0070555 response to interleukin-1
GO:0006936 muscle contraction
GO:0035456 response to interferon-beta
D
Genes commonly regulated by thermoneutrality
logFC
Aspg
Ccdc69
Cebpb
Cyp2b10
Dio2
Gk
Impdh1
Kcnk3
Mgll
Nocl
Orm3
Sh3pxd2a
Slva1
Slc25a34
Slc4a4
Smim4
Snord13
Ucp1
Ucp3
Zfp36l2
E
Genes regulated in GHRfl/fl at 30ºC vs 22ºC
Genes regulated in AgRPΔGHR at 30ºC vs 22ºC
-log10 (FDR)
log2(fold change)
Down
NS
Up
F
AgRPΔGHR at 22ºC
GHRfl/fl at 30ºC vs 22ºC
AgRPΔGHR at 30ºC vs 22ºC
logFC
Gene

Figure 5

SUPPLEMENTARY MATERIAL

Growth hormone receptor (GHR) in AgRP neurons regulates thermogenesis in aged mice in a sex-specific manner

[1#]Lukas Stilgenbauer, [1#]Juliana Bezerra Medeiros de Lima, [1]Lucas Kniess Debarba, [1]Manal Khan, [1]Lisa Koshko, [2]John J. Kopchick, [3]Andrzej Bartke, [4]Augusto Schneider, *[1]Marianna Sadagurski

[1]Department of Biological Sciences, IBio (Integrative Biosciences Center), Wayne State University, Detroit, Michigan, MI, USA.
[2]Edison Biotechnology Institute, Ohio University, Athens, OH, USA
[3]Department of Internal Medicine, Southern Illinois University School of Medicine, Springfield, USA.
[4]Nutrition College, Federal University of Pelotas, Rio Grande do Sul, Brazil.

Running title: Hypothalamic growth hormone signaling controls body core temperature

Keywords: growth hormone receptor; thermoregulation; aging; AgRP neurons

[#] LS and JBL contributed equally to this study

***Corresponding author:**
Marianna Sadagurski,
Department of Biological Sciences,
Integrative Biosciences Center
Wayne State University
6135 Woodward, Detroit, MI 48202
Phone: (313) 577 8637
Email: sadagurski@wayne.edu

Supplementary Figures

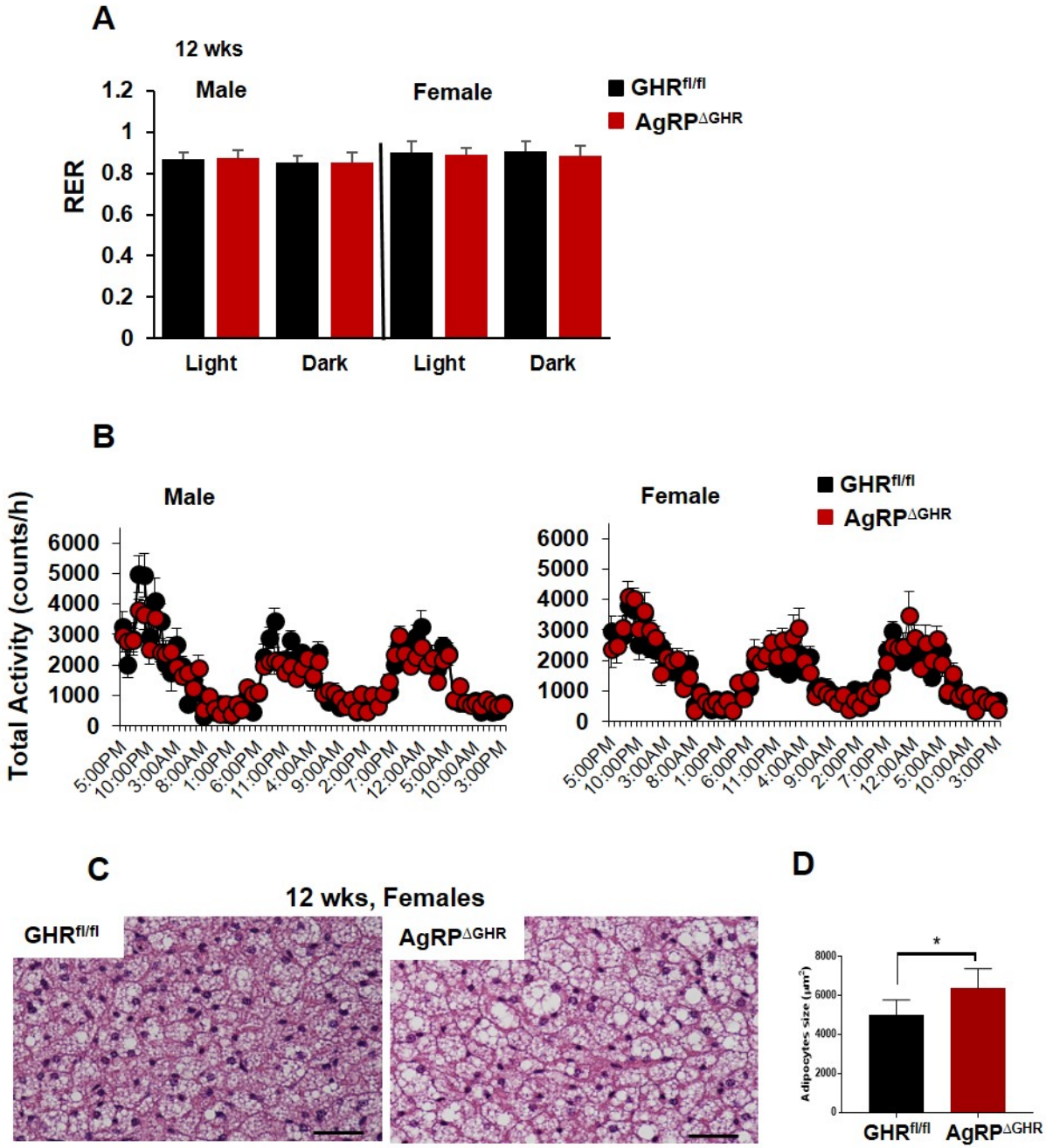

Supplementary Figure 1: Energy homeostasis parameters in 12-week-old control and AgRP$^{\Delta GHR}$ male and female mice. (A) RER (B) Total locomotor activity. (C) Representative H&E staining of brown adipose tissue (BAT) of control (left panel) and AgRP$^{\Delta GHR}$ female mice (right panel) (n=6). Data are shown as mean ± SEM. *, $p<0.005$. Data relates to Figure 1

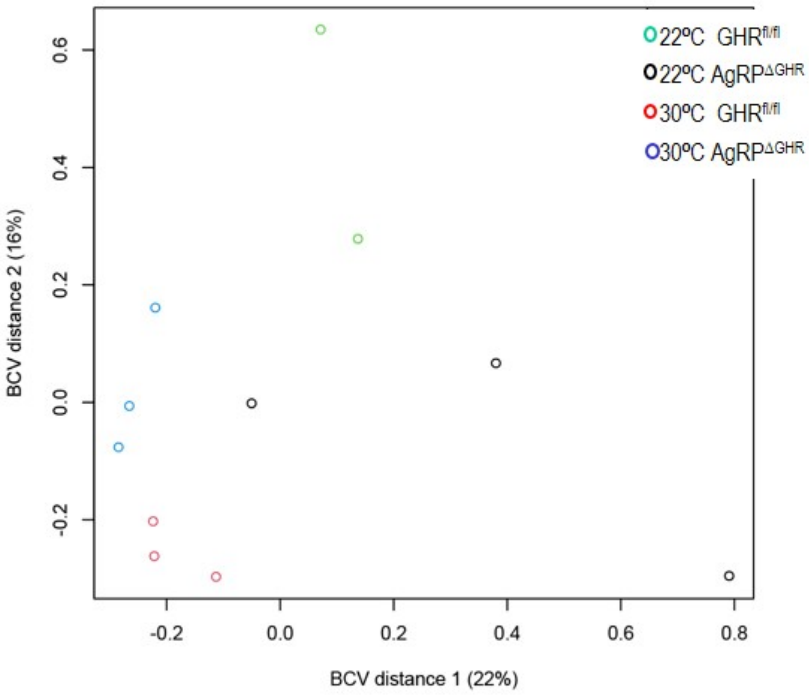

Supplementary Figure 2: Principal components analysis of the most variable expressed mRNAs in brown adipose tissue (BAT). Control and AgRP$^{\Delta GHR}$ female mice at 22ºC and at 30 ºC

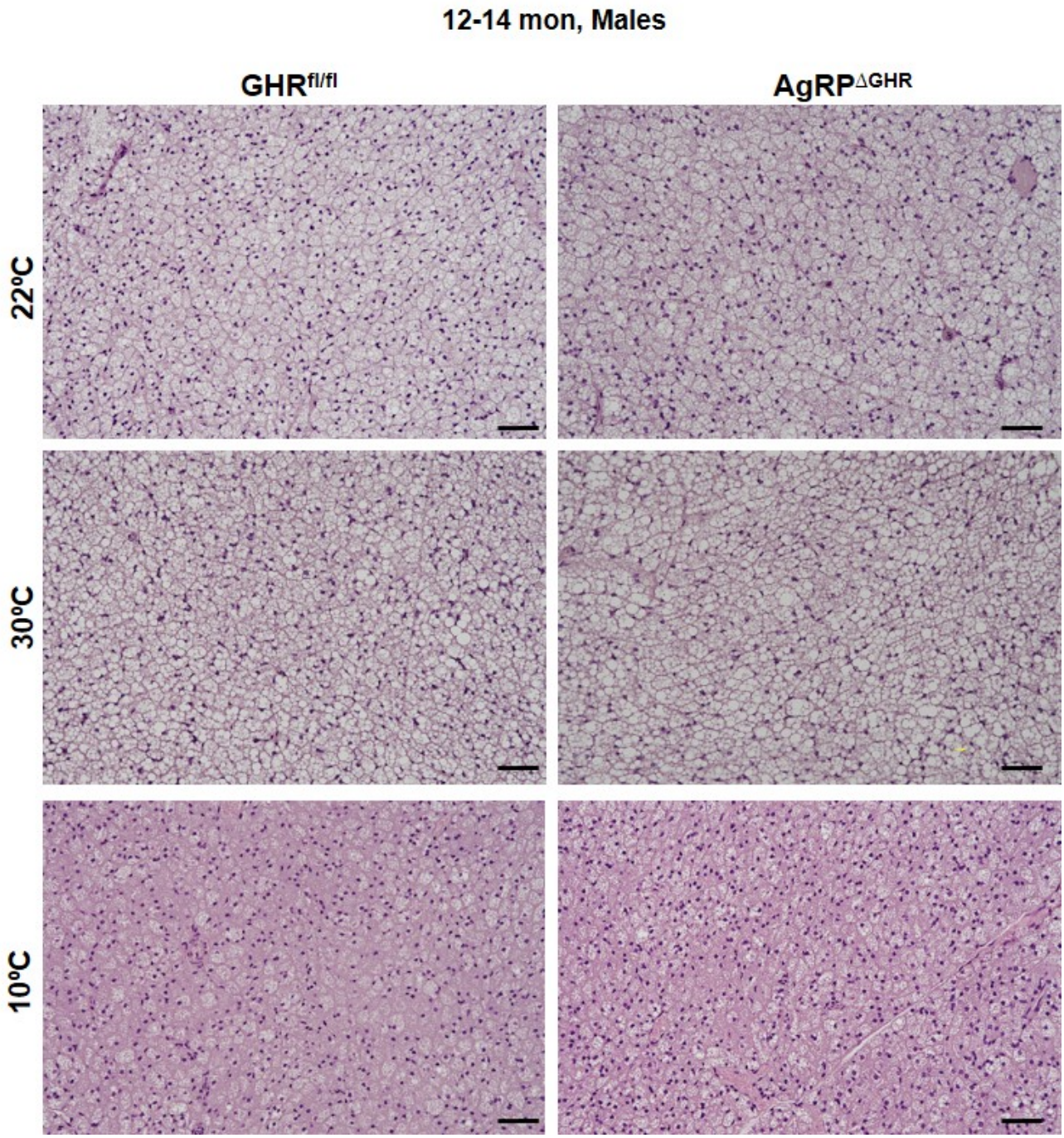

Supplementary Figure 3: Energy homeostasis parameters in 12-week-old control and AgRP$^{\Delta GHR}$ male and female mice. (A) RER (B) Total locomotor activity. (C) Representative H&E staining of brown adipose tissue (BAT) of control (left panel) and AgRP$^{\Delta GHR}$ female mice (right panel) (n=6). Data are shown as mean ± SEM. *, $p<0.005$. Data relates to Figure 3

Supplemental tables

Suppl. Table 1- Enrichment of gene ontology terms in BAT from AgRP$^{\Delta GHR}$ mice at 22°

Up-regulated pathways

Gene Ontology Term	stat.mean	p.val	set.size
GO:0006936 muscle contraction	3.119619244	0.0010326	106
GO:0003012 muscle system process	3.097990741	0.0010821	130
GO:0006941 striated muscle contraction	2.530767889	0.006455	52
GO:0030162 regulation of proteolysis	2.403338183	0.0085592	110
GO:0003009 skeletal muscle contraction	2.540872475	0.0094113	12
GO:0000087 M phase of mitotic cell cycle	2.34170981	0.0098333	212
GO:0000278 mitotic cell cycle	2.267124803	0.0118353	377
GO:0000280 nuclear division	2.187888077	0.0146253	208
GO:0007067 mitosis	2.187888077	0.0146253	208
GO:0043269 regulation of ion transport	2.048231049	0.0206223	191
GO:0048246 macrophage chemotaxis	2.155019339	0.0231232	10
GO:0045730 respiratory burst	2.045034528	0.0260053	15
GO:0019882 antigen processing and presentation	1.97045295	0.0262751	38
GO:0055008 cardiac muscle tissue morphogenesis	1.973540709	0.0263477	35
GO:0007599 hemostasis	1.921803152	0.0284444	65
GO:0003229 ventricular cardiac muscle tissue developmer	1.924595097	0.0299225	28
GO:0022403 cell cycle phase	1.879032259	0.0303014	406
GO:0030193 regulation of blood coagulation	1.914369626	0.0305161	28
GO:1900046 regulation of hemostasis	1.914369626	0.0305161	28
GO:0034622 cellular macromolecular complex assembly	1.874454594	0.0306666	325
GO:0070527 platelet aggregation	1.931371622	0.0333779	12
GO:0042116 macrophage activation	1.849299186	0.0352915	26
GO:0007596 blood coagulation	1.809669177	0.0364078	63
GO:0002690 positive regulation of leukocyte chemotaxis	1.832528609	0.0365526	28
GO:0051310 metaphase plate congression	1.886725811	0.0369213	11
GO:0034109 homotypic cell-cell adhesion	1.807347665	0.038373	26
GO:0002688 regulation of leukocyte chemotaxis	1.80038477	0.0385802	32
GO:0060415 muscle tissue morphogenesis	1.78851146	0.0390591	37
GO:0048285 organelle fission	1.752107358	0.040227	226
GO:0070838 divalent metal ion transport	1.716639379	0.0435578	151
GO:0050818 regulation of coagulation	1.734251735	0.0439241	33
GO:0050808 synapse organization	1.719808449	0.0439937	63
GO:0001881 receptor recycling	1.754026594	0.0443713	19
GO:0000279 M phase	1.693650431	0.045436	291
GO:0050921 positive regulation of chemotaxis	1.707620278	0.0456153	48
GO:0050879 multicellular organismal movement	1.727343503	0.0461242	20

Down-regulated pathways

Gene Ontology Term	stat.mean	p.val	set.size
GO:0045017 glycerolipid biosynthetic process	-2.595904405	0.00514117	86
GO:0035886 vascular smooth muscle cell differentiation	-2.745767026	0.00556219	15
GO:0060947 cardiac vascular smooth muscle cell differentiatic	-2.77343342	0.00782219	10
GO:0018022 peptidyl-lysine methylation	-2.428613536	0.00935177	27
GO:0043414 macromolecule methylation	-2.299929762	0.01118315	116
GO:0046486 glycerolipid metabolic process	-2.19197109	0.01454796	164
GO:0032259 methylation	-2.155308956	0.01590187	181
GO:0006639 acylglycerol metabolic process	-2.083923298	0.01974172	56
GO:0046460 neutral lipid biosynthetic process	-2.056678996	0.02288641	23
GO:0046463 acylglycerol biosynthetic process	-2.056678996	0.02288641	23
GO:0060135 maternal process involved in female pregnancy	-2.052958702	0.02390544	19
GO:0001676 long-chain fatty acid metabolic process	-2.023087261	0.02408639	28
GO:0046850 regulation of bone remodeling	-2.05951003	0.0249426	18
GO:0045684 positive regulation of epidermis development	-2.104206403	0.02574621	11
GO:0030856 regulation of epithelial cell differentiation	-1.953278639	0.02730301	40
GO:0060322 head development	-1.871245204	0.03344894	32
GO:0031018 endocrine pancreas development	-1.90274865	0.03351959	16
GO:0008654 phospholipid biosynthetic process	-1.839083542	0.03371082	100
GO:0034101 erythrocyte homeostasis	-1.835951819	0.03408132	85
GO:0006641 triglyceride metabolic process	-1.837787218	0.03459438	49
GO:0034381 plasma lipoprotein particle clearance	-1.872857614	0.03489831	19
GO:0034968 histone lysine methylation	-1.833486574	0.03494843	51
GO:0006479 protein methylation	-1.818133855	0.03541029	87
GO:0008213 protein alkylation	-1.818133855	0.03541029	87
GO:0009214 cyclic nucleotide catabolic process	-1.915470794	0.0359626	10
GO:0008209 androgen metabolic process	-1.896086573	0.036246	11
GO:0044728 DNA methylation or demethylation	-1.81553716	0.0369948	34
GO:0046474 glycerophospholipid biosynthetic process	-1.795872348	0.03750014	64
GO:0006305 DNA alkylation	-1.820428175	0.03754082	25
GO:0006306 DNA methylation	-1.820428175	0.03754082	25
GO:0007398 ectoderm development	-1.913056254	0.03776789	10
GO:0006661 phosphatidylinositol biosynthetic process	-1.797329584	0.03823457	40
GO:0030902 hindbrain development	-1.782906856	0.03877391	57

Gene Ontology Term	stat.mean	p.val	set.size
GO:0006638 neutral lipid metabolic process	-1.776911103	0.03915268	57
GO:0045682 regulation of epidermis development	-1.786199504	0.04138943	23
GO:0003281 ventricular septum development	-1.759983	0.04190336	31
GO:0030032 lamellipodium assembly	-1.758098491	0.04197924	34
GO:0070585 protein localization to mitochondrion	-1.761858857	0.04206038	30
GO:0007281 germ cell development	-1.738846391	0.04214267	71
GO:0018958 phenol-containing compound metabolic process	-1.751209035	0.04290537	27
GO:0030218 erythrocyte differentiation	-1.722406034	0.04354782	77
GO:0009948 anterior/posterior axis specification	-1.732505526	0.04496997	24
GO:0060412 ventricular septum morphogenesis	-1.724932924	0.04626777	21
GO:0035924 cellular response to vascular endothelial growth fa	-1.727861261	0.04754236	19
GO:0072655 establishment of protein localization to mitochond	-1.700661099	0.04764589	29
GO:0018205 peptidyl-lysine modification	-1.673219504	0.04769255	144
GO:0006839 mitochondrial transport	-1.67918291	0.04782234	63
GO:0003279 cardiac septum development	-1.673552813	0.04919143	40
GO:0019432 triglyceride biosynthetic process	-1.686279161	0.04982814	21

Supplemental tables

Suppl. Table 2- Enrichment of gene ontology terms in BAT from $GHR^{fl/fl}$ mice at 30° vs 22°

Gene Ontology Term	stat.mean	p.val	set.size
GO+AM8:AN69:0009792 embryo development ending in birth o	-3.052621452	0.00117381	384
GO:0043009 chordate embryonic development	-3.038293545	0.00123078	380
GO:0032787 monocarboxylic acid metabolic process	-3.00985783	0.00137615	250
GO:0044255 cellular lipid metabolic process	-2.970528477	0.001526	458
GO:0001676 long-chain fatty acid metabolic process	-3.118083452	0.00156367	28
GO:0051094 positive regulation of developmental process	-2.825793896	0.00241341	427
GO:0044728 DNA methylation or demethylation	-2.915723655	0.00254199	34
GO:0042089 cytokine biosynthetic process	-2.827613218	0.00283433	51
GO:0042107 cytokine metabolic process	-2.827613218	0.00283433	51
GO:0006631 fatty acid metabolic process	-2.691379963	0.00371318	203
GO:0006814 sodium ion transport	-2.645928122	0.00461277	62
GO:0046486 glycerolipid metabolic process	-2.60781095	0.00476823	164
GO:0008610 lipid biosynthetic process	-2.522027413	0.00596581	295
GO:0055006 cardiac cell development	-2.583063988	0.00611592	33
GO:0042692 muscle cell differentiation	-2.511877824	0.00617256	235
GO:0048589 developmental growth	-2.477265539	0.00687238	165
GO:0000038 very long-chain fatty acid metabolic process	-2.619026924	0.00711614	18
GO:0045597 positive regulation of cell differentiation	-2.456010696	0.0071572	320
GO:0003281 ventricular septum development	-2.518378194	0.00734158	31
GO:0055013 cardiac muscle cell development	-2.498758352	0.00782091	28
GO:0006304 DNA modification	-2.458163859	0.00819136	40
GO:0030510 regulation of BMP signaling pathway	-2.456032149	0.00819245	41
GO:0042035 regulation of cytokine biosynthetic process	-2.442370536	0.00837048	43
GO:0034333 adherens junction assembly	-2.435197086	0.00925443	36
GO:0009409 response to cold	-2.639218281	0.00929541	10
GO:0043414 macromolecule methylation	-2.367006033	0.00939146	116
GO:0022612 gland morphogenesis	-2.354426592	0.01008473	63
GO:0006305 DNA alkylation	-2.40281389	0.01044047	25
GO:0006306 DNA methylation	-2.40281389	0.01044047	25
GO:0009887 organ morphogenesis	-2.312529858	0.01050358	394
GO:0090322 regulation of superoxide metabolic process	-2.531160225	0.01081729	11
GO:0006639 acylglycerol metabolic process	-2.327492392	0.01088924	56
GO:0045017 glycerolipid biosynthetic process	-2.315810912	0.0108925	86

Gene Ontology Term	stat.mean	p.val	set.size
GO:0009719 response to endogenous stimulus	-2.296427571	0.01093383	479
GO:0007507 heart development	-2.282121324	0.01142506	287
GO:0016568 chromatin modification	-2.259919639	0.01206971	359
GO:0055007 cardiac muscle cell differentiation	-2.27441235	0.01265898	46
GO:1901342 regulation of vasculature development	-2.247015448	0.01285224	104
GO:0045926 negative regulation of growth	-2.214729994	0.01387258	120
GO:0001701 in utero embryonic development	-2.197799082	0.0142069	256
GO:0051146 striated muscle cell differentiation	-2.194085821	0.01443971	179
GO:0040029 regulation of gene expression, epigenetic	-2.203576196	0.01447207	89
GO:0007044 cell-substrate junction assembly	-2.236659214	0.01471746	37
GO:0006325 chromatin organization	-2.175560479	0.01495064	392
GO:0048878 chemical homeostasis	-2.16498183	0.01532633	449
GO:0016054 organic acid catabolic process	-2.177388287	0.01534225	100
GO:0046395 carboxylic acid catabolic process	-2.177388287	0.01534225	100
GO:0009952 anterior/posterior pattern specification	-2.164994828	0.01576892	107
GO:0008654 phospholipid biosynthetic process	-2.144522815	0.01662763	100
GO:0030509 BMP signaling pathway	-2.141741966	0.01716367	60
GO:0009791 post-embryonic development	-2.135282411	0.01723088	74
GO:0048598 embryonic morphogenesis	-2.119143784	0.01725696	287
GO:0048568 embryonic organ development	-2.119376471	0.0173538	193
GO:0051149 positive regulation of muscle cell differentiation	-2.14927494	0.0177457	34
GO:0048041 focal adhesion assembly	-2.1534683	0.01842325	31
GO:0040007 growth	-2.084905588	0.01867036	483
GO:0051155 positive regulation of striated muscle cell different	-2.170752306	0.01916582	16
GO:0035725 sodium ion transmembrane transport	-2.163797034	0.01958308	15
GO:0014823 response to activity	-2.155004412	0.02033129	14
GO:0002009 morphogenesis of an epithelium	-2.044199677	0.0207516	231
GO:0019752 carboxylic acid metabolic process	-2.020020571	0.02183555	475
GO:0048732 gland development	-2.021040785	0.02212684	140
GO:0071495 cellular response to endogenous stimulus	-2.010588127	0.02237966	347
GO:0030514 negative regulation of BMP signaling pathway	-2.085412861	0.02265728	22
GO:0045844 positive regulation of striated muscle tissue devel	-2.092540737	0.02280069	15
GO:0048636 positive regulation of muscle organ development	-2.092540737	0.02280069	15

Gene Ontology Term	stat.mean	p.val	set.size
GO:1901863 positive regulation of muscle tissue development	-2.092540737	0.02280069	15
GO:0060429 epithelium development	-2.001574921	0.02287164	328
GO:0048705 skeletal system morphogenesis	-2.008142564	0.02301604	99
GO:0003012 muscle system process	-1.997002668	0.02343765	130
GO:0006641 triglyceride metabolic process	-2.012202831	0.02350198	49
GO:0007218 neuropeptide signaling pathway	-2.06543397	0.02352869	18
GO:0032941 secretion by tissue	-2.006977405	0.02427698	37
GO:0055001 muscle cell development	-1.966661145	0.02519219	120
GO:0034103 regulation of tissue remodeling	-2.003298272	0.02541449	25
GO:0006638 neutral lipid metabolic process	-1.966210233	0.02589957	57
GO:0030258 lipid modification	-1.949523933	0.02628225	106

Suppl. Table 3- Enrichment of gene ontology terms in BAT from AgRP$^{\Delta GHR}$ mice at 30°vs 22°

Gene Ontology Term	stat.mean	p.val	set.size
GO:0006325 chromatin organization	-2.272750379	0.01165907	392
GO:0016568 chromatin modification	-2.149459978	0.0159719	359
GO:0051056 regulation of small GTPase mediated signal trans	-2.143727659	0.01629126	230
GO:0007266 Rho protein signal transduction	-2.04966631	0.02092573	92
GO:0006882 cellular zinc ion homeostasis	-2.175643554	0.02205032	10
GO:0055069 zinc ion homeostasis	-2.175643554	0.02205032	10
GO:0060350 endochondral bone morphogenesis	-2.030942362	0.02431471	22
GO:0006637 acyl-CoA metabolic process	-1.989269522	0.02523296	41
GO:0035383 thioester metabolic process	-1.989269522	0.02523296	41
GO:0007265 Ras protein signal transduction	-1.940530929	0.02658181	167
GO:0051276 chromosome organization	-1.867425485	0.03107361	485
GO:0046578 regulation of Ras protein signal transduction	-1.84903222	0.03258235	209
GO:0016071 mRNA metabolic process	-1.846848203	0.03261362	328
GO:0045944 positive regulation of transcription from RNA polyr	-1.841977075	0.0328983	468
GO:0051568 histone H3-K4 methylation	-1.882024158	0.03310752	28
GO:0043576 regulation of respiratory gaseous exchange	-1.945530803	0.0337513	10
GO:0071214 cellular response to abiotic stimulus	-1.831258696	0.03452422	77
GO:0010811 positive regulation of cell-substrate adhesion	-1.841054414	0.03462512	42
GO:0000038 very long-chain fatty acid metabolic process	-1.875335906	0.03527631	18
GO:0051310 metaphase plate congression	-1.901821235	0.03587092	11
GO:0030258 lipid modification	-1.795879951	0.03697851	106
GO:0060349 bone morphogenesis	-1.811164171	0.037039	39
GO:0006814 sodium ion transport	-1.801676724	0.03711173	62
GO:0040029 regulation of gene expression, epigenetic	-1.792304896	0.03740501	89
GO:0001881 receptor recycling	-1.834722711	0.03747828	19
GO:0010608 posttranscriptional regulation of gene expression	-1.762124219	0.03931694	271
GO:0035458 cellular response to interferon-beta	-1.807395593	0.03977913	18
GO:0019395 fatty acid oxidation	-1.724654221	0.04365222	58
GO:0000375 RNA splicing, via transesterification reactions	-1.713839884	0.04431454	79
GO:0070555 response to interleukin-1	-1.732001629	0.04496747	28
GO:0000377 RNA splicing, via transesterification reactions with	-1.69005115	0.04656134	78
GO:0000398 mRNA splicing, via spliceosome	-1.69005115	0.04656134	78
GO:0035456 response to interferon-beta	-1.716756352	0.0468849	21